

# PREDICTING $V_{OC}$ AT ULTRA-HIGH SOLAR CONCENTRATION USING COMPUTATIONAL NUMERICAL ANALYSIS

Margaret Stevens<sup>1</sup>, Chandler Downs<sup>1</sup>, David Emerson<sup>2</sup>, James Adler<sup>2</sup>, Scott Maclachlan<sup>3</sup>, and Thomas E. Vandervelde<sup>1</sup>

<sup>1</sup>The Renewable Energy and Applied Photonics Laboratories, Department of Electrical and Computer Engineering

<sup>2</sup>Department of Mathematics

Tufts University, 161 College Avenue, Medford, MA 02155, USA

<sup>3</sup>Department of Mathematics and Statistics, Memorial University, St. John's, NL, A1C 5S7, Canada

**ABSTRACT:** Under ultra-high solar concentration, drastic efficiency drops are attributed to a deteriorating fill factor and additional thermal effects. The effects of ultra-high solar concentration on other fundamental electrical properties, such as open-circuit voltage, have yet to be explored in detail. In this work, we discuss our theoretical examination of semiconductor performance under ultra-high irradiance. Using advanced numerical analysis techniques and the finite-element library deal.II, we develop a computational model to simultaneously solve the carrier continuity equations and Poisson's equation for optically generated charge carriers and the resulting electric potential as functions of space and time. We use this model to analyze  $V_{OC}$  in both dynamic and quasi-steady state conditions. Ultimately, we characterize the relationship between  $V_{OC}$  and increasing solar concentration.

**Keywords:** III-V semiconductors, concentrator cells, modeling, numerical simulation.

## 1 INTRODUCTION

Today, record efficiencies from concentrated photovoltaic devices (CPVs) emerge from devices subjected to solar concentration greater than 500 suns [1]. In the ultra-high solar concentration regime, the incident light on a photovoltaic device becomes greater than 1000 times the sun. At such high solar concentrations, the magnitude of optically generated carriers begin to rival equilibrium carrier densities, moving devices out of the "low-injection" and towards the "high-injection" regime. This complicates our understanding of carrier dynamics, as drift rivals diffusion for the dominant type of carrier transport in the PN-junction [2].

As a result, understanding complex electrical parameters, such as open-circuit voltage, is a nontrivial challenge. Conventionally, the relationship between open-circuit voltage ( $V_{OC}$ ) and solar concentration ( $X$ ) is linked to the diode ideality factor ( $n$ ).

$$V_{oc} = \frac{nkT}{q} \ln \left( \frac{I_{sc}(X)}{I_0} + 1 \right) \quad (1)$$

$$\approx V_{oc}^{\{1\text{ sun}\}} + \frac{nkT}{q} \ln(X)$$

Although Equation 1 is experimentally confirmed at under high irradiance ( $X < 1000$  suns), this explanation breaks down under ultra-high irradiance ( $X > 1000$  suns). In the logarithmic plots depicted in Figure 1, the flattening slope of  $V_{OC}(X)$  is attributed to non-radiative or Auger recombination dominating [4][5]. Any sublinear behavior of  $V_{OC}(X)$  under ultra-high irradiance has been dismissed as cell overheating [5]; however, sublinear behavior is still present under conventional flash-testing where the duration of illumination is short and, therefore, should not generate significant thermal effects [5]. This inconsistency reveals a gap in our understanding of  $V_{OC}$ 's dependence on solar concentration.

To predict  $V_{OC}$  at ultra-high solar concentrations, we utilize the definitions of the quasi-Fermi levels to model  $V_{OC}$  under quasi-steady state and dynamic conditions.

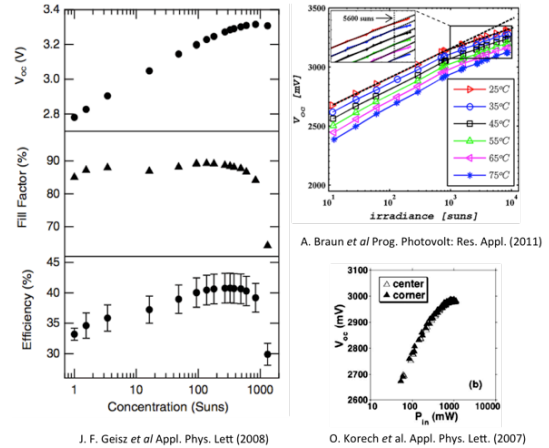


**Figure 1:** (a) Triple junction GaInP/InGaAs/InGaAs CPV subjected to high-irradiance flash testing [3]. (b) Dual junction GaInP/GaInAs/Ge CPV subjected to ultra-high irradiance flash testing [5]. (c) Triple junction GaInP/GaAs/Ge CPV subjected constant ultra-high irradiance [6].

$$E_{F_n}(x, t) = E_i + kT \ln \left( \frac{n(x, t)}{n_i} \right) \quad (2)$$

$$E_{F_p}(x, t) = E_i - kT \ln \left( \frac{p(x, t)}{n_i} \right) \quad (3)$$

$$V_{oc}(t) = E_{F_n} - E_{F_p} = \frac{kT}{q} \ln \left( \frac{n(x_p, t)p(x_n, t)}{n_i^2} \right) \quad (4)$$

Equation 4 yields a definition of  $V_{OC}$  that is directly related to the charger carrier distributions in space and time. Typically, the splitting of the quasi-Fermi levels is considered to be constant across the depletion region and steadily increasing with solar concentration, a valid assumption in the low-injection regime. However, as mentioned before, low-injection assumptions may no longer hold under ultra-high solar concentration. In this

work, we simultaneously solve the carrier continuity equations and Poisson's equation in space and time without many of the standard simplifying assumptions to investigate the effect of dynamically changing carrier concentrations on the splitting of the quasi-Fermi levels, and ultimately  $V_{OC}$ .

## 2 PROBLEM FORMULATION

The carrier continuity equations characterize the flux of electrons ( $n$ ) and holes ( $p$ ) through a semiconductor. We solve these two equations simultaneously with Poisson's equation, which determines the electric potential that arises from the carrier distributions. In 1D, our partial-differential equation (PDE) system is as follows

$$\frac{\partial n}{\partial t} = \frac{1}{q} \frac{\partial}{\partial x} \left( q D_n \frac{\partial n}{\partial x} + q \mu_n n \frac{\partial V}{\partial x} \right) + G_{op}(x) - U, \quad (5)$$

$$\frac{\partial p}{\partial t} = \frac{1}{q} \frac{\partial}{\partial x} \left( q D_p \frac{\partial p}{\partial x} - q \mu_p p \frac{\partial V}{\partial x} \right) + G_{op}(x) - U, \quad (6)$$

$$\frac{\partial^2 V}{\partial x^2} = - \frac{q(p - n + N_D - N_A)}{\epsilon}, \quad (7)$$

where  $D_n$ ,  $D_p$ ,  $\mu_n$ ,  $\mu_p$ , and  $\epsilon$  are material parameters. In this work, we chose to model a gallium arsenide (GaAs) solar cell; therefore, we chose parameters appropriate for this condition. Our charge carrier distributions,  $n(x,t)$  and  $p(x,t)$  can be thought of as the superposition of equilibrium carriers and excess, optically generated, carriers.

$$n(x, t) = n_0 + \delta n(x, t) \quad (8)$$

$$p(x, t) = p_0 + \delta p(x, t) \quad (9)$$

### 2.1 Generation and Recombination

We consider a spatially varying generation profile for optically generated carriers based on the Beer-Lambert Law, rather than the simplified uniformly illuminated condition. Light intensity and generated carriers both decay as a function of depth through the semiconducting material at a rate determined by the absorption coefficient,  $\alpha$ . Our generation profile has the following form,

$$G_{op} = \alpha X L_f e^{-\alpha x}, \quad (10)$$

where  $\alpha$  and the photon flux ( $L_f$ ) are material parameters chosen to model GaAs.

The net recombination rate ( $U$ ) considered in this work is comprised of radiative and Auger recombination: the dominating recombination types under low and high-irradiance,

$$U = R_{ec}(np - n_i^2) + (A_n n + A_p p)(np - n_i^2), \quad (11)$$

where  $R_{ec}$  is the radiative recombination constant and  $A_n/A_p$  are the Auger constants for GaAs.

### 2.2 Boundary Conditions

To achieve a unique solution to our PDE system we impose boundary conditions (BCs) on our unknowns ( $n$ ,  $p$ ,  $V$ ) at  $x=0$  and  $x=L$ , the total depth of the semiconducting material. The BCs imposed on the carrier distributions are Robin, in that they constrain the derivative of the function to its value at that point. This arises from surface recombination effects.

$$\frac{\partial n}{\partial x} \Big|_{x=0} = \frac{S_r}{D_n} (n(0) - n_0) \quad (12)$$

$$\frac{\partial n}{\partial x} \Big|_{x=L} = - \frac{S_r}{D_n} (n(L) - n_0) \quad (13)$$

$$\frac{\partial p}{\partial x} \Big|_{x=0} = \frac{S_r}{D_p} (p(0) - p_0) \quad (14)$$

$$\frac{\partial p}{\partial x} \Big|_{x=L} = - \frac{S_r}{D_p} (p(L) - p_0) \quad (15)$$

The boundary conditions for the electric potential,  $V$ , can be either Dirichlet (function value is imposed on boundary) or Neumann (derivative value is imposed on boundary). We began with Dirichlet BCs, as we know  $V(L)$  is determined by the built-in-voltage of the PN-junction,

$$V(0) = 0 \quad (16)$$

$$V(L) = \frac{kT}{q} \ln \left( \frac{N_A N_D}{n_i^2} \right) \quad (17)$$

where  $N_A$  and  $N_D$  are the doping profiles of the p-type and n-type material, respectively.

### 2.3 Finite-Element Method (FEM)

To solve our PDE system, we created a flexible computational model that uses finite-element methods (FEM) and nested iteration to numerically approximate solutions to a linearized, variational formulation of our original system [7]. Our process employs the Newton-Raphson method: an iterative process that approximates the root of a real function. The process in its simplest form is as follows,

$$0 = f_k'(x) \Delta x + f_k(x) \quad (18)$$

$$f_{k+1}(x) = f_k(x) + \Delta x. \quad (19)$$

In our problem, we simultaneously solve for the roots of Equations 5-7 by calculating the iterative updates ( $\Delta n$ ,  $\Delta p$ ,  $\Delta V$ ) that bring us closer to the true solutions.

### 2.4 Nondimensionalization

To manage the widely varying orders of magnitudes present in our problem, we utilize a nondimensionalization scheme based on the Debye length of a charge carrier [9]. Here,

$$x_0 = \sqrt{\frac{\epsilon k T}{q^2 N}} \quad (20)$$

where  $N$  is of the same order of magnitude as the dopant concentrations,  $N_A$  or  $N_D$ .

We employ these techniques together in deal.II, an open-source FEM library that facilitates solving complicated PDE systems [9]. We eliminate any second-order terms by integrating by parts and applying the Robin BCs, yielding a first-order variational system. We build our solutions using Lagrange elements of order 2, scaled to define our functions over the material depth  $L=1\mu\text{m}$ .

### 3 RESULTS

#### 3.1 Quasi-Steady State Condition: High Concentration

We began by zeroing the time derivatives in Equations 5-7 to investigate  $V_{OC}$  in the quasi-steady state condition. This allows us to solve our PDE system spatially, rather than both spatially and temporally. Figure 2 shows the concentration carrier profiles and resulting band structure under  $V_{OC}$  conditions while illuminated by 1 sun. We observe conventional splitting of the quasi-Fermi levels. Under high solar concentration ( $X=1000$ ), the magnitude of minority carriers increases, resulting in a larger split between the quasi-Fermi levels.

#### 3.2 Time-stepping Considerations

To solve our PDE system temporally, we introduce time-stepping and a second nondimensionalization scheme. We scale our time steps by the dielectric relaxation time scale [9], which is related to the Debye length as follows.

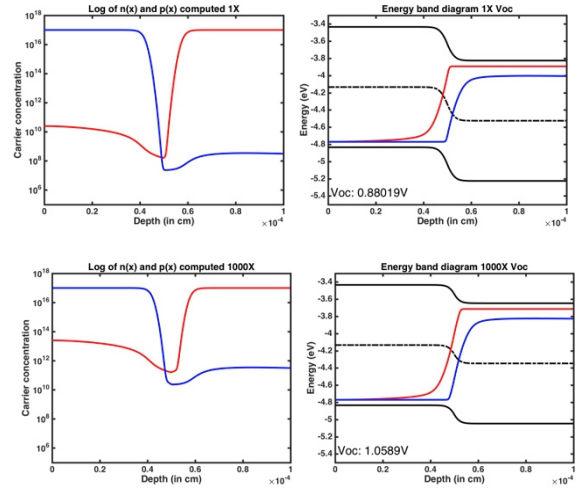
$$\tau_0 = \frac{\chi_0^2}{D_n} \quad (21)$$

Figure 3 depicts the time-evolution of excess carriers after the generation source is turned off at  $t=0$ . The minority carriers rapidly decay to their equilibrium values, with the electrons reaching the equilibrium value quicker than the holes. This is due to the large difference in mobility between electrons and holes in GaAs. We intend to use this version of the solver to simulate “flash-testing” conditions.

#### 3.3 Ultra-High Concentration and $V_{OC}$ Effects

As we increase solar concentration up to 100,000 suns, we observe a steady increase in  $V_{OC}$ . Figure 4 shows that this increase is linear, and is identical with and without Auger recombination accounted for in our net recombination rate ( $U$ ). The inset in Figure 4 shows that Auger recombination does not outpace radiative recombination in GaAs until carrier densities are  $>10^{21} \text{ cm}^{-3}$ . This would seem to show that carrier dynamics do not cause a drop-off in  $V_{OC}$  at ultra-high concentration.

However, when we look at the carrier profiles at concentrations that would “wash-out” the PN-junction effects –  $\delta n \gg n_0$  in the n-type material, or  $\delta p \gg p_0$  in the p-type material – we notice unusual behavior. Figure 5 depicts the carrier concentration profiles and electric potential under 100,000,000 suns solar concentration. At this concentration, the optically generated carriers are an order of magnitude greater than the equilibrium majority carriers. We see that the total electron and hole densities are almost equal in the p-type region of the device, resulting in a near zero electric potential. However, in the n-type portion of the device the profiles return to the



**Figure 2:** Carrier concentration profiles and energy band diagrams under 1X and 1000X. Electrons and the electron quasi-Fermi level are represented by the red lines, while the holes and hole quasi-Fermi level are represented by the blue lines.  $V_{OC}$  is calculated to be the maximum split between the quasi-Fermi levels on the band diagram.

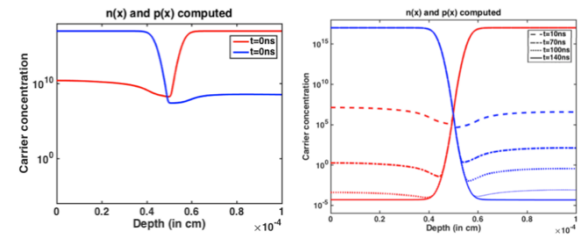


**Figure 3:** Time evolution of optically generated carriers decaying to equilibrium concentrations.

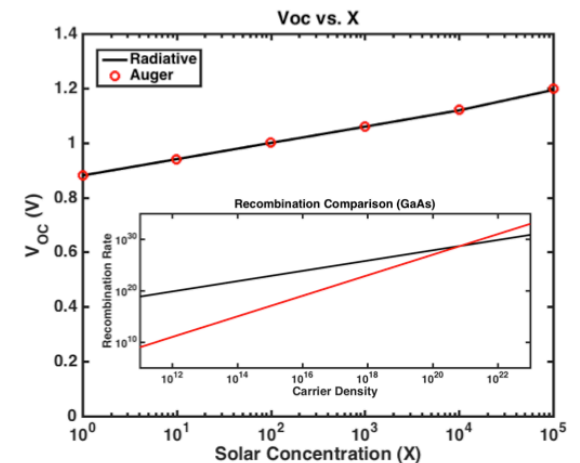


**Figure 4:** (a)  $V_{OC}$  plotted logarithmically against increasing solar concentration ( $X$ ). Plots with and without Auger recombination are identical up to 100,000 suns, which is consistent with the inset plot, showing that Auger recombination does not outpace radiative recombination until carrier densities are of order  $10^{21} \text{ cm}^{-3}$ .

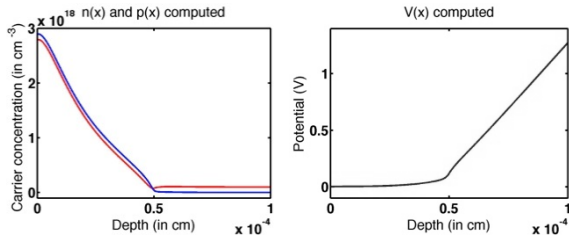


**Figure 5:** Computed carrier and potential profiles for  $X=100,000,000$  suns. Dirichlet BCs are forcing PN-junction behavior where it should be washed out.

same values that were present in the PN-junction, and the electric potential increases linearly to the built-in voltage, set by our Dirichlet BC. We believe this to be an artificial effect, rather than a result of the carrier dynamics. Therefore, it is possible that we are not seeing the true evolution of  $V_{OC}$  with solar concentration, and rather are seeing a trend that is a result of enforcing the Dirichlet boundary condition.

In a conventional PN-junction, the electric field ( $\xi$ ) is only nonzero in the depletion region. Therefore, we can employ zero Neumann BCs on the electric potential.

$$\xi(0) = \frac{\partial V}{\partial x} \Big|_{x=0} = 0 \quad (22)$$

$$\xi(L) = \frac{\partial V}{\partial x} \Big|_{x=L} = 0 \quad (23)$$

However, in order to achieve a unique solution to Poisson's equation in this manner, we must uphold the compatibility condition [7].

$$\int_0^L \frac{q(p(x,t) - n(x,t) + N_D - N_A)}{\epsilon} = 0 \quad (24)$$

As this is a global constraint, it is computationally expensive to implement into our solver. We are currently exploring other ways of satisfying this condition without drastically slowing computation time.

#### 4 CONCLUSIONS

In this work, we solved a PDE system that governs the spatial dependence of charge carriers and the electric potential in ultra-high concentration photovoltaics. Using the deal.II finite-element library, we computed carrier density profiles for a variety of solar concentrations illuminating a GaAs PN-junction, and solved for the resulting  $V_{OC}$ . Additionally, we integrated time-stepping into our solver in order to model flash testing conditions. We demonstrate a linear relationship between  $V_{OC}$  and solar concentration, but note that this may be a result of our strongly enforced boundary condition on the electric potential, rather than a result of carrier dynamics. In future work, we will implement zero Neumann boundary conditions on the electric potential to more accurately characterize the evolution of  $V_{OC}$  with increasing solar concentration.

#### 5 REFERENCES

- [1] M.A. Green, K. Emery, Y. Hishikawa, W. Warta, and E.D. Dunlop "Solar cell efficiency tables (version 46)". *Prog. Photovolt: Res. Appl.*, 23, (2015), 805–812.
- [2] M. Stevens, C. Downs, D. Emerson, J. Adler, S. Maclachlan, T.E. Vandervelde "Studying Anomalous Open-Circuit Voltage Drop-Out in Concentrated Photovoltaics Using Computational Numerical Analysis" *Photovoltaic Specialists Conference (PVSC), 2015 42nd IEEE*. New Orleans, June 14-19, 2015
- [3] J. F. Geisz et al. "40.8% efficient inverted triple-junction solar cell with two independently metamorphic junctions." *Appl. Phys. Lett.* 93 123505 (2008).
- [4] A. Vossier, B. Hirsch, J. M. Gordon "Is Auger recombination the ultimate performance limiter in concentrator solar cells?" *Appl. Phys. Lett.* 97, 193509 (2010).
- [5] A. Braun, B. Hirsch, A. Vossier, E. A. Katz, J. M. Gordon, "Temperature dynamics of multijunction concentrator solar cells up to ultra-high irradiance." *Prog. Photovolt.: Res. Appl.* 21, (2) (2013) 202-208.
- [6] O. Korech, B. Hirsch, E. A. Katz, J. M. Gordon, "High-flux characterization of ultrasmall multijunction concentrator solar cells" *Appl. Phys. Lett.* 91 064101 (2007)
- [7] S. C. Brenner and R. Scott, *The Mathematical Theory of Finite Element Methods* 3rd ed. New York, NY: Springer, 2008
- [8] D. Vasileska, S. M. Goodnick, and G. Klimeck. *Computational Electronics: Semiclassical and Quantum Device Modeling and Simulation*. Taylor and Francis Group, 2010.
- [9] W. Bangerth, R. Hartmann, G. Kanschat, "deal.II- A general-purpose object-oriented finite element library." *ACM Trans. Math. Softw.* 33, (4) (2007) 24/1-24/27